Journal of Magnetism and Magnetic Materials 369 (2014) 223–227

Contents lists available at ScienceDirect

Journal of Magnetism and Magnetic Materials

journal homepage: www.elsevier.com/locate/jmmm

Interaction between 3*d*-, 4*d*- and 5*d*-electron in $Sr_2Ir_{1-x}(Ru,Ti)_xO_4$

Min Ge [a], Shun Tan [a,*], Jifeng Shao [a], Li Pi [a,b], Yuheng Zhang [a,b]

[a] Hefei National Laboratory for Physical Sciences at the Microscale, University of Science and Technology of China, Hefei 230026, China
[b] High Magnetic Field Laboratory, Chinese Academy of Sciences, Hefei 230031, China

ARTICLE INFO

Article history:
Received 21 August 2013
Received in revised form
10 May 2014
Available online 25 June 2014

Keywords:
Spin–orbit coupling
Micromagnetism

ABSTRACT

The effect of substituting 3*d*-nonmagnetic Ti^{4+} and 4*d*-magnetic Ru^{4+} for 5*d*-magnetic Ir^{4+} in Sr_2IrO_4 polycrystals has been studied. The magnetic transition temperature T_N decreases with Ru doping, while T_N is almost unchanged with Ti doping. This phenomenon indicates that there is super-exchange coupling between Ir^{4+} and Ru^{4+}, which is weaker than that of Ir–O–Ir, while there is no interaction between Ir^{4+} and Ti^{4+}. The resistivity of $Sr_2Ir_{1-x}Ru_xO_4$ decreases with increasing x due to the introduction of holes upon Ru doping, and the ρ–T relation presents the percolation phenomenon in $0.31 \leq x \leq 0.6$ range. On the contrary, the resistivity of $Sr_2Ir_{1-x}Ti_xO_4$ increases with x. The increase of ρ is attributed to the scattering of additional vibration modes of Sr_2TiO_4 in which are measured by IR spectra.

1. Introduction

The 5*d*-electron based iridates have attracted considerable attention due to the interaction between strong spin–orbit coupling and other correlation interactions such as electron correlation and electron–phonon interaction [1–34]. It is known that the relativistic spin–orbit interaction proportional to Z^4 (where Z is the atomic number) ranges from 0.2 to 1 eV in 5*d* materials (as compared to ~20 meV in 3*d* materials), which is comparable to the Coulomb interaction U on-site (0.5–2 eV). So, the competition between the spin–orbit coupling with Coulomb and other energies is subtle in 5*d* materials, and the balance will be broken when 3*d* and 4*d* atoms are introduced.

The layered perovskite Sr_2IrO_4 crystallizes in a reduced tetragonal structure with space-group $I4_1/acd$. The IrO_6 octahedra rotate around the *c*-axis about 11° in the unit cell, which plays a key role in determining the electronic structure [16,19,24]. Sr_2IrO_4 is a weak ferromagnetic insulator [6] and the Mott insulating gap between upper and lower Hubbard bands in the $J_{eff}=1/2$ bands is induced by the Coulomb repulsion U (about 0.5 eV) [7]. The theoretical calculation predicts that it has a possibility to be a high temperature superconductor if doped [20,24,26,30,31]. Therefore, interesting properties are anticipated in the doped Sr_2IrO_4 compound [20]. Sr_2TiO_4 is a paramagnetic insulator and Sr_2RuO_4 is a superconductor [3]. As we know, Ti belongs to the 3*d*-electron system and Ru belongs to the 4*d*-electron system. The balance of several interactions is broken in some different degrees. Then it is necessary to investigate the interaction among 3*d*-, 4*d*- and 5*d*-electron through substituting Ir^{4+} with Ru^{4+} and Ti^{4+} in Sr_2IrO_4.

In this work, we investigate the polycrystalline sample Sr_2IrO_4, $Sr_2Ir_{1-x}Ru_xO_4$ and $Sr_2Ir_{1-x}Ti_xO_4$ by the X-ray diffractometer, electron magnetic resonance (EMR), infrared (IR), transport and measurements of macroscopic magnetism. Our experimental results show that there is interaction between Ru^{4+} and Ir^{4+}. The magnetic transition temperature T_N is suppressed and the resistivity decreases greatly with Ru doping. The percolation phenomenon is observed when $0.3 \leq x \leq 0.6$. For $Sr_2Ir_{1-x}Ti_xO_4$, the magnetic moment decreases with Ti doping and T_N is almost the same with Sr_2IrO_4, which indicates that there is no interaction between Ti^{4+} and Ir^{4+}. The resistivity of Ti doped compounds is enhanced dramatically since the appearance of many vibration modes in $Sr_2Ir_{1-x}Ti_xO_4$. The different electromagnetic behaviors of $Sr_2Ir_{1-x}(Ru,Ti)_xO_4$ are analysed.

2. Experiment

Polycrystalline samples of $Sr_2Ir_{1-x}Ru_xO_4$ and $Sr_2Ir_{1-x}Ti_xO_4$ (x=0–0.8) were prepared by the solid-state reaction method. The starting materials, powders of $SrCO_3$ (purity 99.9%), IrO_2 (99.9%), RuO_2 (99.99%) and TiO_2 (99.9%) were mixed uniformly according to the stoichiometric ratio. The mixed powder samples were heated to 1103 K in air. After holding for 24 h, the samples were cooled down to room temperature. Then the powder samples were ground and pressed into round-shaped pellets and heat treated at 1273 K for another two days.

* Corresponding author.
E-mail address: tans@ustc.edu.cn (S. Tan).

http://dx.doi.org/10.1016/j.jmmm.2014.06.030
0304-8853/

Structure and phase purities were checked by the Rigaku-TTR3 X-ray diffractometer using high-intensity graphite monochromatized Cu Kα radiation at room temperature. The magnetization was measured using a superconducting quantum interference device (SQUID) magnetometer. The EMR spectra were recorded using an electron spin resonance (ESR) spectrometry in the X-band at the microwave frequency of 9.4 GHz. The resistivity measurements were performed by the conventional four-probe method using a Physical Property Measurement System (Quantum Design PPMS). The infrared transmission spectra were obtained (Bruker Vertex 80v) by using powder samples with CsI serving as a carrier.

3. Results and discussion

Fig. 1 shows powder X-ray diffraction (XRD) patterns for $Sr_2Ir_{1-x}Ru_xO_4$ and $Sr_2Ir_{1-x}Ti_xO_4$ ($x=0$, 0.1, 0.6) at room temperature. Single phase patterns were obtained at all values of x. For Sr_2IrO_4, $Sr_2Ir_{0.9}Ru_{0.1}O_4$ and $Sr_2Ir_{0.9}Ti_{0.1}O_4$, their Bragg diffractions could be assigned to a tetragonal cell with the space group $I4_1/acd$. The diffraction peaks for $x=0.1$ samples move toward higher angle direction compared with that of Sr_2IrO_4, which is due to the smaller size of Ru^{4+} and Ti^{4+}. However, their lattice symmetry remains unchanged. For $Sr_2Ir_{0.4}Ru_{0.6}O_4$ and $Sr_2Ir_{0.4}Ti_{0.6}O_4$, their diffraction patterns show clear differences from Sr_2IrO_4. For example, the indistinguishable (0,0,12) and (1,1,10) peaks for Sr_2IrO_4 are replaced by three peaks (1,0,5), (0,0,6) and (1,1,4) for $x=0.6$ samples in 41–45° 2θ range. They can be indexed with the symmetry of space group $I4/mmm$, which is an ideal K_2NiF_4-type structure. Therefore, the lattice symmetry is changed at very high doping.

Fig. 2 depicts the temperature dependence of magnetization for $Sr_2Ir_{1-x}Ru_xO_4$ and $Sr_2Ir_{1-x}Ti_xO_4$ ($x=0$–0.8) under the magnetic field of 0.2 T. For pure Sr_2IrO_4, there is a sharp magnetic transition at approximately 240 K, which has been reported to be introduced by the Dzyaloshinskii–Moriya (DM) interaction [2–5,8,6,16,24]. The magnetic ground state of Sr_2IrO_4 is a canted antiferromagnetic state, which produces a residual ferromagnetic component in the IrO_2 planes. The origin of canted antiferromagnetic state is the Dzyaloshinskii–Moriya (DM) interaction derived from the spin–orbit coupling with the rotation of IrO_6 octahedra [14,15]. With the doping of Ru in Sr_2IrO_4, T_N decreases rapidly and the sample shows paramagnetic behavior when $x \geq 0.4$, as described in Fig. 2(a). For $Sr_2Ir_{1-x}Ti_xO_4$, as is shown in Fig. 2(b), the magnetic moment decreases rapidly with Ti doping, while T_N is almost unchanged

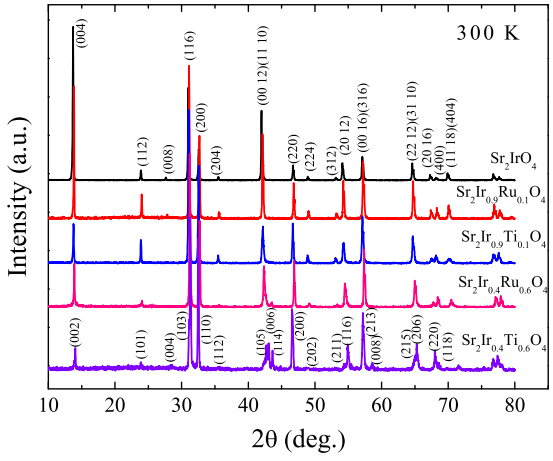

Fig. 1. Powder X-ray diffraction (XRD) patterns for Sr_2IrO_4, $Sr_2Ir_{0.9}Ru_{0.1}O_4$, $Sr_2Ir_{0.9}Ti_{0.1}O_4$, $Sr_2Ir_{0.4}Ru_{0.6}O_4$, and $Sr_2Ir_{0.4}Ti_{0.6}O_4$ at room temperature.

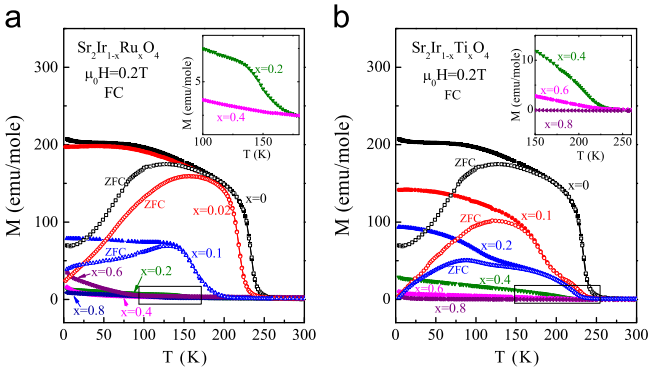

Fig. 2. Temperature dependence of the magnetization $M(T)$ for (a) $Sr_2Ir_{1-x}Ru_xO_4$ and (c) $Sr_2Ir_{1-x}Ti_xO_4$ measured under 0.2 T. The inset is the enlargement of rectangular part in FC processes.

with x. When $x=0.1$ and 0.2, the magnetic moment is enhanced below 190 K and 120 K respectively. But this behavior disappears when $x \geq 0.4$. Comparing $M(T)$ in ZFC and FC processes, it is found that clusters are introduced upon Ti doping. We will discuss this phenomenon in the following part of IR experiment. It is obvious that there is super-exchange interaction between Ru^{4+} and Ir^{4+}. Thus T_N decreases with doping Ru in Sr_2IrO_4. On the other hand, the substitution of Ir^{4+} with Ti^{4+} seems to only affect the magnitude of susceptibility without participating in the interaction of Ir–O–Ir. Therefore, T_N is nearly unchanged with doping Ti in Sr_2IrO_4.

To explore the magnetic transition in Ru and Ti doped samples, the micromagnetism in two systems was further investigated by EMR. Fig. 3 shows the differential EMR spectra (dP/dH) of Sr_2IrO_4, $Sr_2Ir_{0.9}Ru_{0.1}O_4$ and $Sr_2Ir_{0.9}Ti_{0.1}O_4$ measured at selected temperatures from 300 K to 2 K.

As depicted in Fig. 3(a), the EMR spectra can be separated into three typical temperature regions. In the first temperature range from 300 K to 230 K, no EMR signal is observed. The temperature region from 220 K to 40 K is defined as the middle temperature region, where the EMR line appears at 220 K. Then a strong intensity of EMR line is observed at the resonance field H_s (defined as H_s at $dP/dH=0$) of 0.079 T at 210 K. The EMR line located at 0.079 T is attributed to the canted magnetic order with $J_{eff}=1/2$ in Sr_2IrO_4 below the magnetic transition temperature [35]. Then the ferromagnetic resonance field shifts to higher field, as shown in Fig. 3(a). Meanwhile, the reduction of EMR line intensity with the decreasing temperature is obviously induced by a decreased Boltzmann population difference between the two energy levels. In the third temperature region from 40 K to 2 K, although the EMR signals are very weak below 40 K, H_s increases slightly with the decreasing temperature.

For $Sr_2Ir_{0.9}Ru_{0.1}O_4$, we observed a strong intensity of EMR line when the temperature decreases to 120 K. It is corresponding to the end of transition from PM to FM, as shown in Fig. 2(a). But the resonance field at 120 K is higher than that of Sr_2IrO_4 at 210 K. Then the intensity of EMR line decreases with temperature. Meanwhile, the line position of EMR line also shifts to higher magnetic field similar to Sr_2IrO_4. The EMR spectra of $Sr_2Ir_{1-x}Ru_xO_4$ ($x \geq 0.2$) were also measured, but we cannot observe any EMR line. This phenomenon indicates that the magnetism of Ru^{4+} cannot be measured by EMR, because the spin–lattice relaxation is so strong that the half-width of the EMR signals is too broad to be observed. The EMR lines measured in $Sr_2Ir_{0.9}Ru_{0.1}O_4$ is attributed to the super-exchange interaction of Ir–O–Ir. When 10% Ru is doped into Sr_2IrO_4, the Ir–O–Ir interaction is suppressed by Ir–O–Ru, so the appearance of EMR line decreases from 220 K to 120 K.

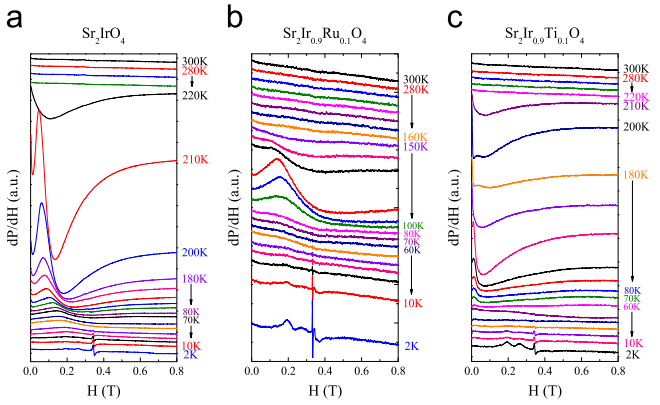

Fig. 3. The differential EMR spectra (dP/dH) of (a) Sr_2IrO_4, (b) $Sr_2Ir_{0.9}Ru_{0.1}O_4$, and (c) $Sr_2Ir_{0.9}Ti_{0.1}O_4$ at selected temperatures from 300 K to 2 K.

For $Sr_2Ir_{0.9}Ti_{0.1}O_4$, a strong intensity of EMR line appears at 210 K, which is almost the same with Sr_2IrO_4. But the resonance field H_s is apparently smaller than that of Sr_2IrO_4 and we can barely observe a whole Lorenz line. With the decreasing temperature, the intensity of EMR line decreases progressively with temperature until 60 K, while H_s keeps almost unchanged with the decreasing temperature. As we know, there is no interaction between Ti^{4+} and Ir^{4+}, the EMR signals are introduced by Ir–O–Ir interaction. Through the differences of EMR spectra between Sr_2IrO_4 and $Sr_2Ir_{0.9}Ti_{0.1}O_4$, their internal fields determined by the Ir–O–Ir interaction are different. It is apparent that the internal field of $Sr_2Ir_{0.9}Ti_{0.1}O_4$ is higher than Sr_2IrO_4, and the Ir–O–Ir interaction in $Sr_2Ir_{0.9}Ti_{0.1}O_4$ is stronger than in Sr_2IrO_4. These discrepancies will be discussed below.

For Sr_2IrO_4 and $Sr_2Ir_{0.9}(Ru,Ti)_{0.1}O_4$, the weak intensities of EMR lines with $g\sim2$ are observed from 40 K to 2 K, which might be produced by a tiny amount of unreacted raw material-IrO_2 [35]. The micromagnetic results are in agreement with the results which we obtained through the macromagnetic measurements.

Fig. 4 shows the temperature dependence of resistivity in (a) $Sr_2Ir_{1-x}Ru_xO_4$ and (d) $Sr_2Ir_{1-x}Ti_xO_4$ under magnetic field of 0 T, which exhibit the insulating behavior through the whole temperature range from 300 K to 2 K. There is no transition in $\rho(T)$ curves at the magnetic transition temperature, which indicates that ρ is not effected by the PM–FM transition. The resistivity decreases greatly with doping Ru in Sr_2IrO_4. Ru doping adds holes, giving rise to a higher density of state near E_F and hence supporting a more metallic state comparing with Sr_2IrO_4. Conversely, the resistivity of $Sr_2Ir_{1-x}Ti_xO_4$ increases drastically with x, and it cannot be measured when x exceeds 0.4. Because there is no interaction between Ir^{4+} and Ti^{4+}, and Ti^{4+} just blocks the Ir–O–Ir interaction.

Then we study further the conductive mechanism of $Sr_2Ir_{1-x}(Ru,Ti)_xO_4$. Firstly, it is found that the transport properties cannot be described with either thermal activation or three-dimensional variable-range hopping mode (VRH) for $Sr_2Ir_{1-x}(Ru,Ti)_xO_4$, as can be seen in Fig. 4(b), (c), (e) and (f). However, VRH seems to fit much better than the thermal activation mode. It is interesting that the $\ln\rho\sim1/T$ and $\ln\rho\sim(1/T)^{1/4}$ relation of $Sr_2Ir_{1-x}Ru_xO_4$ can be classified into three kinds, as shown in Fig. 4(e) and (f). For $x=0$-0.2, the resistivity increases rapidly with the decreasing temperature and shows semiconductor-like behavior. Furthermore, it is shown that the VRH mode corresponds well to experimental results, as can be seen in Fig. 4(f). For $x=0.31$–0.6, the $\ln\rho\sim1/T$ and $\ln\rho\sim(1/T)^{1/4}$ curves also present semiconductor-like behavior, but the resistivity increases rather slowly with cooling. For $x=0.8$, the resistivity is relatively small

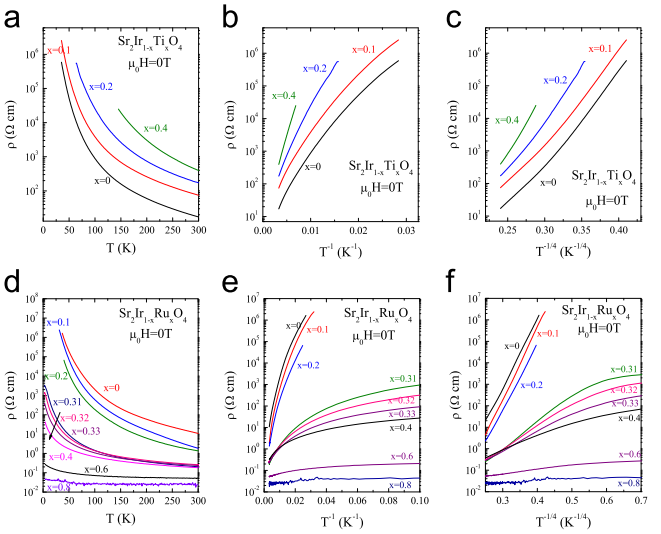

Fig. 4. Temperature dependence of resistivity $\rho(T)$ for (a) $Sr_2Ir_{1-x}Ti_xO_4$ and (d) $Sr_2Ir_{1-x}Ru_xO_4$ measured under 0 T. Plotted $\ln\rho\sim1/T$ (b), (e) and $\ln\rho\sim(1/T)^{1/4}$ (c), (f) curves for $Sr_2Ir_{1-x}Ti_xO_4$ and $Sr_2Ir_{1-x}Ru_xO_4$ respectively.

and it shows almost linear behavior with $1/T$ and $(1/T)^{1/4}$. However, neither the thermal activation nor VRH itself can depict the transport behaviors of $Sr_2Ir_{1-x}Ru_xO_4$. It seems that $x=0.31$ is the threshold value of $Sr_2Ir_{1-x}Ru_xO_4$. When $x<0.3$, the resistivity increases rapidly with the decreasing temperature. Ru^{4+} ions act as the scatterers in Sr_2IrO_4, even though ρ decreases with increasing x. The Ru–O–Ru channel is formed when $x\geq0.31$, which is favorable for the conduction of Sr_2RuO_4. Therefore, the percolation phenomenon emerges in $Sr_2Ir_{1-x}Ru_xO_4$ systems. Considering pure Sr_2IrO_4, the resistivity can be described approximatively with $\rho_{Ir}=\rho_1\exp(T_0/T)^{1/4}$. Sr_2RuO_4 exhibits superconductivity in the single-crystalline form with significant anisotropy in its electrical properties [36]. For polycrystalline Sr_2RuO_4, the electrical data are not conclusive and it shows semiconducting behavior [37], so its resistivity is nearly $\rho_{Ru}=\rho_2\exp(E_g/kT)$. When x increases to 0.31, there are two channels, Ir–Ir and Ru–Ru, which are in parallel to each other. Then the total resistivity of $0.31\leq x\leq0.6$ can be described as

$$\rho=\frac{\rho_{Ir}\times\rho_{Ru}}{\rho_{Ir}+\rho_{Ru}} \quad (1)$$

According to this model, the resistivity curves have been fitted in Fig. 5, in which raw data (dotted lines) are in accordance with fitting curves (solid lines) quite well. The obtained parameters are shown in Table 1. They are reasonable and regular.

In order to clear the origin of different behaviors in transport and magnetization for Ru and Ti doped systems, we investigated the lattice dynamics of $Sr_2Ir_{1-x}(Ru,Ti)_xO_4$ by the infrared spectra.

Fig. 6 depicts the IR transmission spectra for (a) Sr_2IrO_4, (b) $Sr_2Ir_{0.9}Ru_{0.1}O_4$ and (c) $Sr_2Ir_{0.9}Ti_{0.1}O_4$ at selected temperatures from 5 K to 300 K. As we know, the crystal structure of Sr_2IrO_4 is D_{4h}^{20}–$I4_1/acd$, which is derived from a distorted K_2NiF_4 ($I4/mmm$)-type tetragonal structure [32]. In Fig. 6(a), five modes are observed, which are classified into external and bending modes. As can be seen, the change in the phonon modes with the decreasing temperature is smooth and no clear split of phonon modes is observed, indicating the absence of a structural transition [17,32].

For $Sr_2Ir_{0.9}Ru_{0.1}O_4$, as can be seen in Fig. 6(b), five peaks are also observed from 300 K to 140 K. However, when the temperature decreases to 120 K, the peak located at about 400 cm^{-1}, which

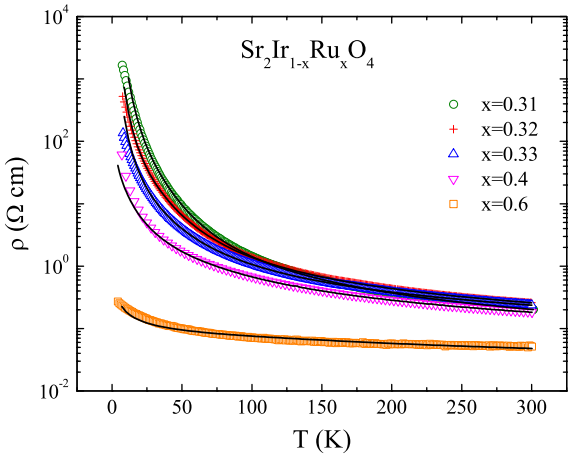

Fig. 5. Temperature dependence of resistivity for $Sr_2Ir_{1-x}Ru_xO_4$ ($x=0.31$–0.6). Dots are experimental data, and lines are fitting curves corresponding to our model.

Table 1
Parameters of $Sr_2Ir_{1-x}Ru_xO_4$ ($0.31 \le x \le 0.6$) obtained from resistivity fitting.

x	ρ_1 (10^{-3} Ω cm)	T_0 (K)	ρ_2 (Ω cm)	E_g (k)
0.31	0.493	436 773.89	0.59	248.44
0.32	1.77	235 663.53	0.42	252.02
0.33	2.81	147 980.19	0.33	305.19
0.4	6.11	50 242.25	0.22	452.18
0.6	24.3	171.86	0.05	488.19

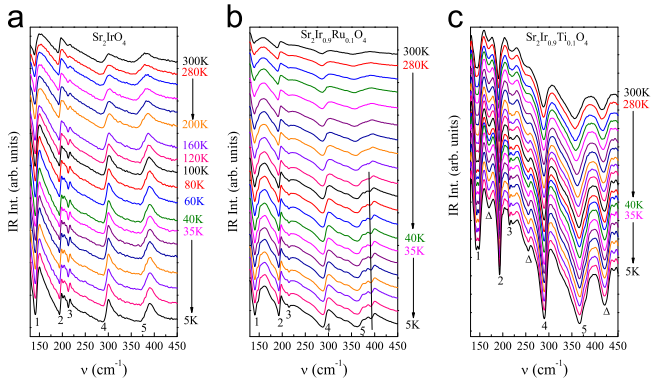

Fig. 6. Temperature-dependent infrared transmission spectra of (a) Sr_2IrO_4, (b) $Sr_2Ir_{0.9}Ru_{0.1}O_4$, and (c) $Sr_2Ir_{0.9}Ti_{0.1}O_4$ at selected temperatures from 300 K to 5 K.

corresponds to the modulation of the Ir–O–Ir bond angle [32], splits into two peaks, indicated by the straight line in Fig. 6(b). This phenomenon indicates that the vibration mode of Ir–O–Ru is observed at low temperature. On the other hand, 120 K is the magnetic transition temperature of $Sr_2Ir_{0.9}Ru_{0.1}O_4$, which is shown in Figs. 2(a) and 3(b). Through the IR spectra, it is clear that there is interaction between Ir^{4+} and doped Ru^{4+}, which is weaker than the interaction among Ir^{4+}. Therefore, the magnetic transition temperature decreases with Ru doping.

When Ti is doped in Sr_2IrO_4, the situation is different from Ru doping. For $Sr_2Ir_{0.9}Ti_{0.1}O_4$, some additional phonon modes are observed, which are marked by triangles in Fig. 6(c). These phonon modes together with the five modes of Sr_2IrO_4 are well assigned to the phonon modes in pure Sr_2TiO_4 [38]. As we know, the vibration peaks of Sr_2TiO_4 cannot appear if 10% Ti is distributed uniformly throughout the sample. The appearance of Sr_2TiO_4 vibration modes indicates that excess Ir–O–Ti vibration exists in $Sr_2Ir_{0.9}Ti_{0.1}O_4$. Therefore, clusters are formed by Ti doping. The long-range ordered Ir–O–Ir interaction would be blocked by Ti, and then it changes to short-range ordered Ir–O–Ir interaction. It is clear that the magnetic transition at 240 K, as shown in Fig. 2(b), is attributed to the long-range ordered Ir–O–Ir interaction. When the temperature decreases to about 190 K, the increase of susceptibility is induced by the short-range ordered Ir–O–Ir interaction. Due to clusters formed by Ti, the canted-AFM of short-range ordered Ir–O–Ir is perturbed and the FM component is enhanced. So, EMR line of $Sr_2Ir_{0.9}Ti_{0.1}O_4$ appears at 210 K and H_s is smaller than that of Sr_2IrO_4, as depicted in Fig. 3(a) and (c). Although the FM component is enhanced in the short-ranged clusters, the long-range ordered Ir–O–Ir interaction is broken by Ti. Then the macro-magnetic moment decreases with Ti doping. As for the transport of $Sr_2Ir_{1-x}Ti_xO_4$, the more modes determine the strength of scattering, and this is the reason for the increase of resistivity with Ti doping.

4. Conclusion

In summary, our experimental results indicate that the magnetic transition temperature of $Sr_2Ir_{1-x}Ru_xO_4$ is suppressed with Ru doping due to the weaker super-exchange interaction of Ir–O–Ru compared with the interaction of Ir–O–Ir. The resistivity decreases with increasing x and we observe the percolation phenomenon when $0.31 \le x \le 0.6$. For $Sr_2Ir_{1-x}Ti_xO_4$, its susceptibility decreases rapidly with increasing x. Through the IR spectra, additional vibration modes are observed, which explains the increase of resistivity with Ti doping. These behaviors show that there is no interaction between Ir^{4+} and Ti^{4+}.

Acknowledgments

This work was supported by the State Key Project of Fundamental Research of China through Grant no. 2010CB923403, the National Natural Science Foundation of China through Grant no. 11204288, the Fundamental Research Funds for the Central Universities WK2340000040, and Postdoctoral Science Foundation of China 2012M521226.

References

[1] G. Cao, Y. Xin, C.S. Alexander, J.E. Crow, P. Schlottmann, M.K. Crawford, R.L. Harlow, W. Marshall, Phys. Rev. B 66 (2002) 214412.
[2] M.K. Crawford, M.A. Subramanian, R.L. Harlow, J.A. Fernandez-Baca, Z.R. Wang, D.C. Johnston, Phys. Rev. B 49 (1994) 9198.
[3] R.J. Cava, B. Batlogg, K. Kiyono, H. Takagi, J.J. Krajewski, W.F. Peck Jr., L.W. Rupp Jr., C.H. Chen, Phys. Rev. B 49 (1994) 11890.
[4] Q. Huang, J.L. Soubeyroux, O. Chmaissem, I. Natali Sora, A. Santoro, R.J. Cava, J.J. Krajewski, W.F. Peck Jr., J. Solid State Chem. 112 (1994) 355.
[5] Tetsuo. Shimura, Yoshiyuki Inaguma, Tetsuro Nakamura, Mitsuru Itoh, Phys. Rev. B 52 (1995) 9143.
[6] G. Cao, J. Bolivar, S. McCall, J.E. Crow, R.P. Guertin, Phys. Rev. B 57 (1998) R11039.
[7] S.J. Moon, M.W. Kim, K.W. Kim, Y.S. Lee, J.-Y. Kim, J.-H. Park, B.J. Kim, S.-J. Oh, S. Nakatsuji, Y. Maeno, I. Nagai, S.I. Ikeda, G. Cao, T.W. Noh, Phys. Rev. B 74 (2006) 113104.
[8] N.S. Kini, A.M. Strydom, H.S. Jeevan, C. Geibel, S. Ramakrishnan, J. Phys.: Condens. Matter 18 (2006) 8205.
[9] T.F. Qi, O.B. Korneta, L. Li, K. Butrouna, V.S. Cao, X. Wan, P. Schlottmann, R.K. Kaul, G. Cao, Phys. Rev. B 86 (2012) 125105.
[10] B.J. Kim, Hosub Jin, S.J. Moon, J.-Y. Kim, B.-G. Park, C.S. Leem, Jaejun Yu, T.W. Noh, C. Kim, S.-J. Oh, J.-H. Park, V. Durairaj, G. Cao, E. Rotenberg, Phys. Rev. Lett. 101 (2008) 076402.
[11] S.J. Moon, H. Jin, K.W. Kim, W.S. Choi, Y.S. Lee, J. Yu, G. Cao, A. Sumi, H. Funakubo, C. Bernhard, T.W. Noh, Phys. Rev. Lett. 101 (2008) 226402.
[12] Y. Klein, I. Terasaki, J. Phys.: Condens. Matter 20 (2008) 295201.
[13] B.J. Kim, H. Ohsumi, T. Komesu, S. Sakai, T. Morita, H. Takagi, T. Arima, Science 323 (2009) 1329.
[14] G. Jackeli, G. Khaliullin, Phys. Rev. Lett. 102 (2009) 017205.

[15] Hosub Jin, Hogyun Jeong, Taisuke Ozaki, Jaejun Yu, Phys. Rev. B 80 (2009) 075112.
[16] S. Chikara, O. Korneta, W.P. Crummett, L.E. DeLong, P. Schlottmann, G. Cao, Phys. Rev. B 80 (2009) 140407(R).
[17] S.J. Moon, Hosub Jin, W.S. Choi, J.S. Lee, S.S.A. Seo, J. Yu, G. Cao, T.W. Noh, Y.S. Lee, Phys. Rev. B 80 (2009) 195110.
[18] H. Watanabe, T. Shirakawa, S. Yunoki, Phys. Rev. Lett. 105 (2010) 216410.
[19] O.B. Korneta, T.F. Qi, S. Chikara, S. Parkin, L.E. DeLong, P. Schlottmann, G. Cao, Phys. Rev. B 82 (2010) 115117.
[20] Fa. Wang, T. Senthil, Phys. Rev. Lett. 106 (2011) 136402.
[21] C. Martins, M. Aichhorn, L. Vaugier, S. Biermann, Phys. Rev. Lett. 107 (2011) 266404.
[22] I. Franke, P.J. Baker, S.J. Blundell, T. Lancaster, W. Hayes, F.L. Pratt, G. Cao, Phys. Rev. B 83 (2011) 094416.
[23] K. Ishii, I. Jarrige, M. Yoshida, K. Ikeuchi, J. Mizuki, K. Ohashi, T. Takayama, J. Matsuno, H. Takagi, Phys. Rev. B 83 (2011) 115121.
[24] M. Ge, T.F. Qi, O.B. Korneta, D.E. DeLong, P. Schlottmann, W.P. Crummett, G. Cao, Phys. Rev. B 84 (2011) 100402(R).
[25] R. Arita, J. Kunes, A.V. Kozhevnikov, A.G. Eguiluz, M. Imada, Phys. Rev. Lett. 108 (2012) 086403.
[26] Jungho Kim, D. Casa, M.H. Upton, T. Gog, Young-June Kim, J.F. Mitchell, M. van Veenendaal, M. Daghofer, J. van den Brink, G. Khaliullin, B.J. Kim, Phys. Rev. Lett. 108 (2012) 177003.
[27] S. Fujiyama, H. Ohsumi, T. Komesu, J. Matsuno, B.J. Kim, M. Takata, T. Arima, H. Takagi, Phys. Rev. Lett. 108 (2012) 247212.
[28] D. Haskel, G. Fabbris, M. Zhernenkov, P.P. Kong, C.Q. Jin, G. Cao, M. Veenendaal, Phys. Rev. Lett. 109 (2012) 027204.
[29] V.M. Katukuri, H. Stoll, J. Brink, L. Hozoi, Phys. Rev. B 85 (2012) 220402(R).
[30] J.S. Lee, Y. Krockenberger, K.S. Takahashi, M. Kawasaki, Y. Tokura, Phys. Rev. B 85 (2012) 035101.
[31] D. Hsieh, F. Mahmood, D.H. Torchinsky, G. Cao, N. Gedik, Phys. Rev. B 86 (2012) 035128.
[32] Mehmet Fatih Cetin, Peter Lemmens, Vladimir Gnezdilov, Dirk Wulferding, Dirk Menzel, Tomohiro Takayama, Kei Ohashi, Hidenori Takagi, Phys. Rev. B 85 (2012) 195148.
[33] B. Fisher, J. Genossar, A. Knizhnik, L. Patlagan, G.M. Reisner, J. Appl. Phys. 101 (2007) 123703.
[34] N. Keawprak, R. Tu, T. Goto, J. Alloys Compd. 491 (2010) 441.
[35] M. Ge, S. Tan, Y. Huang, L. Zhang, W. Tong, L. Pi, Y. Zhang, J. Magn. Magn. Mater. 345 (2013) 13.
[36] Y. Maeno, H. Hashimoto, K. Yoshida, S. Nishizaki, T. Fujita, J.G. Bednorz, F. Lichtenberg, Nature 372 (1994) 532.
[37] R.J. Cava, B. Batlogg, K. Kiyono, H. Takagi, J.J. Krajewski, W.F. Peck Jr., L.W. Rupp Jr., C.H. Chen, Phys. Rev. B 49 (1994) 11890.
[38] Gerald Burns, F.H. Dacol, G. Kliche, W. Konig, M.W. Shafer, Phys. Rev. B 37 (1988) 3381.